Crystal structures of the new ternary stannides $La_3Mg_{4-x}Sn_{2+x}$ and $LaMg_{3-x}Sn_2$

P. Solokha[1*], S. De Negri[1], R. Minetti[1], D.M. Proserpio[2,3], A. Saccone[1]

[1]Università degli Studi di Genova, Dipartimento di Chimica e Chimica Industriale, via Dodecaneso 31, 16146 Genova, Italy

[2]Università degli Studi di Milano, Dipartimento di Chimica, Via Golgi 19, 20133 Milano, Italy

[3]Samara Center for Theoretical Materials Science (SCTMS), Samara State University, Samara 443011, Russia

Abstract

Synthesis and structural characterization of the two new lanthanum-magnesium-stannides $La_3Mg_{4-x}Sn_{2+x}$ ($0.12 \le x \le 0.40$) and $LaMg_{3-x}Sn_2$ ($0.33 \le x \le 0.78$) are reported. The crystal structures of these intermetallics were determined by single crystal X-ray diffraction analysis and confirmed by Rietveld refinement of powder X-ray diffraction patterns of the corresponding samples.

The $La_3Mg_{4-x}Sn_{2+x}$ phase crystallizes in the hexagonal $Zr_3Cu_4Si_2$ structure type ($P\bar{6}2m$, *hP*9, *Z*=3, x = 0.12(1), a = 7.7974(7), c = 4.8384(4) Å), which represents an ordered derivative of the *hP*9-ZrNiAl prototype, ubiquitous among equiatomic intermetallics.

The $LaMg_{3-x}Sn_2$ phase is the second representative of the trigonal $LaMg_{3-x}Ge_2$ type, which is a superstructure of the $LaLi_3Sb_2$ structure type ($P\bar{3}1c$, *hP*34-0.12, *Z*=6, x = 0.35(1), a = 8.3222(9), c = 14.9546(16) Å). The scheme describing the symmetry reduction/colouring with respect to the parent type is reported here with the purpose to discuss the $LaMg_{3-x}Sn_2$ off-stoichiometry from the geometrical point of view.

Structural relationships between the La–Mg–Sn ternary phases, including the already known equiatomic LaMgSn compound (*oP*12-TiNiSi), are presented in the framework of the AlB_2-related compounds family and discussed with the aid of group-subgroup relations in the *Bärnighausen* formalism.

Keywords: Stannides, Crystal structure, Single-crystal X-ray diffraction, Group-subgroup relation, AlB_2-related structures

* Corresponding author. E-mail: pavlo.solokha@unige.it. Phone: +39-0103536159. Fax: +39-0103536163.

1. Introduction

This work is a part of systematic research devoted to the study of phase relations and crystal chemistry in *R*–Mg–*T* ternary systems, where *R* is a rare earth metal and *T* a transition or *p*-block element [1, 2, 3]. In fact, these systems have been proved to be rich of ternary intermetallic phases, studied from the point of view of crystal structure, chemical bonding and physical properties [4, 5, 6, 7]. The structural and chemical role of Mg in such compounds is of special interest: in several cases this element was found to be bonded to the most electronegative component (*T*) to form a polyanionic network counterbalanced by the rare earth metal [6, 7, 8, 9, 10]. In particular, for *T* = tetrel (elements of the 14 group of the periodic table), different structural fragments based on *T*–*T* covalent interactions stabilized by Mg were highlighted [7, 11, 12, 13].

Whereas numerous rare earth-magnesium-germanides have already been studied [3, 7, 12, 13], data on related stannides are practically limited to the RMgSn equiatomic compounds [14]. In fact, the high oxidizability of binary and ternary alloys based on R–Sn systems is an experimental drawback which significantly hampers the research of new compounds. Nevertheless, during our investigation of the La–Mg–Sn system [15] several novel ternary intermetallics were detected and characterized: two of them, $La_3Mg_{4-x}Sn_{2+x}$ and $LaMg_{3-x}Sn_2$, are presented in this paper. Beyond the description of their synthesis and crystal structure solution, the crystallographic similarities between these phases, together with the already known LaMgSn, will be discussed in terms of AlB_2-related structures with the aid of group-subgroup relations in the *Bärnighausen* formalism.

2. Experimental details

Single crystals of $La_3Mg_{4-x}Sn_{2+x}$ and $LaMg_{3-x}Sn_2$ were selected from two alloys of nominal compositions $La_{35.0}Mg_{43.0}Sn_{22.0}$ (sample # 1) and $La_{17.0}Mg_{48.0}Sn_{35.0}$ (sample # 2) respectively.

Pure (≥ 99.9 mass%) constituent metals were used for the direct synthesis; all of them were supplied by NewMet Koch, Waltham Abbey, England. A sealed Ta crucible, containing the stoichiometric amounts of the three elements, was enclosed into an evacuated quartz vial and placed in a resistance furnace equipped with a thermal controller. A thermal cycle was then applied, consisting of a heating from room temperature to 850 °C (sample # 1) or 950 °C (sample # 2) with a rate of 10 °C/min, an isothermal plateau of 2 minutes and finally a slow cooling (about 0.3 °C/min) down to 350 °C. The furnace was then switched off and the alloys were cooled until room temperature. A continuous rotation, at a speed of 100 rpm, was applied to the vial during the thermal cycle: from our experience this procedure favours the growth of good quality crystals.

Microstructure examination as well as qualitative and quantitative analyses were performed on polished samples by a scanning electron microscope (SEM) Zeiss Evo 40 equipped with a Pentafet

Link Energy Dispersive X-ray Spectroscopy (EDXS) system managed by the INCA Energy software (Oxford Instruments, Analytical Ltd., Bucks, U.K.).

Good quality single crystals were extracted from the two mechanically fragmented samples and subsequently mounted on glass fibers using quick-drying glue. The crystals are sufficiently stable in air at ambient conditions to perform standard X-ray diffraction experiments.

A full-sphere dataset was obtained in routine fashion at ambient conditions on a four-circle Bruker Kappa APEXII CCD area-detector diffractometer equipped by the graphite monochromatized Mo Kα radiation (λ = 0.71073 Å). The instrument was operated in the ω-scan mode. The acquired scans (exposure for 20 s per frame) were integrated using *SAINT-Plus* [16] and the highly redundant final dataset was corrected for Lorentz and polarization effects. Semiempirical absorption corrections (SADABS) [16] were applied to all data. The structures were solved by Jana2006 [17] and refined by full-matrix least-squares procedures on $|F^2|$ using the SHELXL programs [18] as implemented in WinGx [19]. No missed higher crystallographic symmetry in the final models was found by PLATON [20]. Refined positional parameters have been standardized by STRUCTURE TIDY program [21]. Details on the structure refinement can be found in the Supporting Information in the form of CIF file. The CIF has also been deposited with Fachinformationszentrum Karlsruhe, 76344 Eggenstein-Leopoldshafen, Germany: depository numbers CSD-429707 ($La_3Mg_{4-x}Sn_{2+x}$), CSD-429708 ($LaMg_{3-x}Sn_2$). Some details of the data collection and refinement for the studied crystals are summarized in Table 1; the structure solution is described in the "Result and discussion" section.

The precession photos of *hk0* zone for $La_3Mg_{4-x}Sn_{2+x}$ and *h0l* zone for $LaMg_{3-x}Sn_2$ single crystals reconstructed from experimental datasets are shown in Fig. 1a-b, respectively.

X-ray powder diffraction data were collected on the two studied samples by means of a vertical diffractometer Philips X'Pert MPD (Philips, Almelo, the Netherlands), using the Cu-Kα radiation at room temperature. The angular range 5-110° was scanned, with step width and time per step suitable to obtain a good peak resolution. Rietveld refinement was subsequently performed, using the Jana2006 or Fullprof softwares [17, 22], in order to ensure the structural models.

The homogeneity regions of the two studied compounds were determined by SEM-EDXS and XRPD analysis of several La-Mg-Sn samples synthesized by induction melting and annealed at 500 °C in order to investigate the corresponding isothermal section [15].

Table 1. Crystallographic data for the $La_3Mg_{4-x}Sn_{2+x}$ and $LaMg_{3-x}Sn_2$ single crystals together with some experimental details of the structure determination.

Empirical formula	$La_3Mg_{4-x}Sn_{2+x}$, x=0.12(1)	$LaMg_{3-x}Sn_2$, x=0.35(1)
Structure type	$Zr_3Cu_4Si_2$	$LaMg_{3-x}Ge_2$
Formula weight, g·mol^{-1}	253.60	441.12
Crystal system	Hexagonal	Trigonal
Space group	*P* $\bar{6}$2*m* (№ 189)	*P* $\bar{3}$1*c* (№ 163)
Pearson symbol, Z	*hP*9, 3	*hP*34-0.12, 6
θ range for data collection, deg	3.0-31.6	2.7-31.6
hkl range	±11, ±11, ±7	±12, ±12, ±21
Unit cell dimensions:		
a, Å	7.7974(7)	8.3222(9)
c, Å	4.8384(4)	14.9546(16)
V, Å^3	254.76(5)	897.0(2)
Calc. density (D_{calc}, g·cm^{-3})	4.959	4.900
Abs. coefficient (μ, mm^{-1})	17.536	15.425
Total no. reflections	6154	20655
Flack parameter	0.06(3)	–
Independent reflections	355 (R_{int} = 0.0473)	1013 (R_{int} = 0.0377)
Reflections with $I > 2\sigma(I)$	339 (R_{sigma} = 0.0207)	719 (R_{sigma} = 0.0135)
Data/parameters	355/16	1013/30
Goodness-of-fit on F^2	1.12	1.05
Final *R* indices; R_1/wR_2	0.0140/0.0165	0.0174/0.0319
R indices (all data)	0.0191/0.0195	0.0338/0.0378
$\Delta\rho_{fin}$ (max/min), e·nm^{-3} (×10^3)	0.58/-0.72	0.75/-0.87

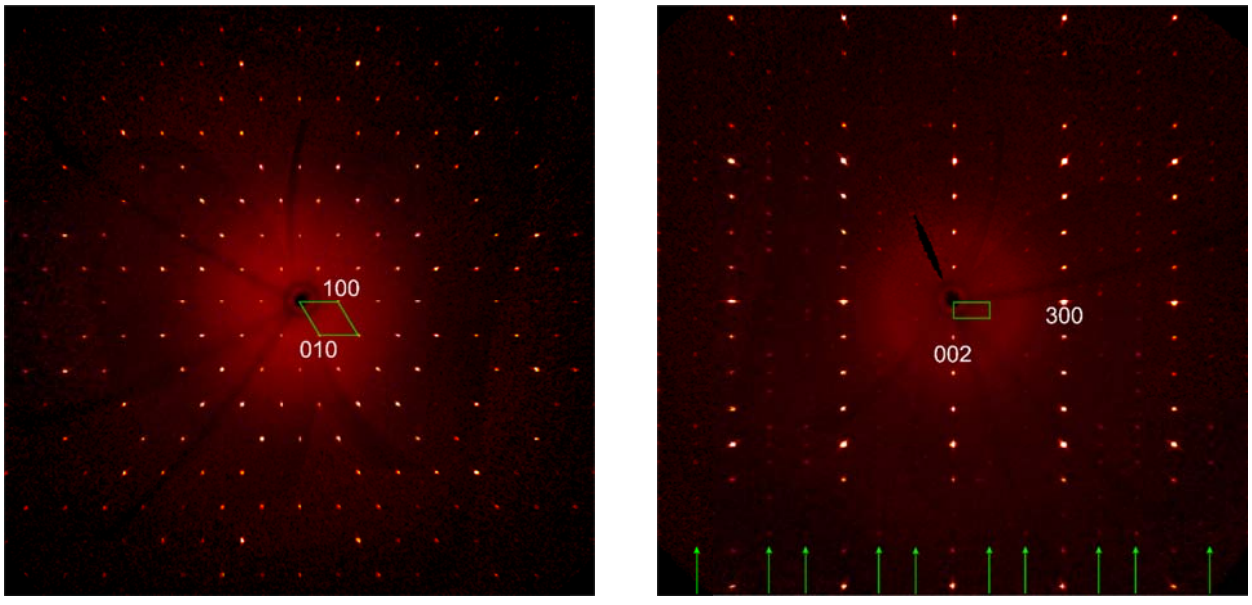

a) b)

Figure 1. Observed intensity profiles of the *hk0* zone for $La_3Mg_{4-x}Sn_{2+x}$ (a) and of the *h0l* zone for $LaMg_{3-x}Sn_2$ (b) reconstructed from experimental single crystal datasets. The reciprocal cells are highlighted in green, and the Miller indices are shown for a few reflections. The weak supercell reflections are indicated by green arrows in the case of $LaMg_{3-x}Sn_2$.

3. Results and discussion

3.1 Sample characterization by SEM-EDXS analysis

The applied synthetic method often leads to inhomogeneous, multi-phase alloys, nevertheless containing large crystals suitable for single crystal X-ray measurements. An appropriate choice of the synthetic conditions, such as nominal composition and thermal cycle, normally allows obtaining a good yield of the compound of interest.

Based on SEM-EDXS analyses, sample # 1 contains a large amount of $La_3Mg_{4-x}Sn_{2+x}$ (measured composition: $La_{35.9}Mg_{40.7}Sn_{23.4}$) coexisting with three secondary phases: a new ternary compound (measured composition: $La_{22.5}Mg_{73.6}Sn_{3.9}$), $LaMg_3$ and LaMgSn. Sample # 2 is almost $LaMg_{3-x}Sn_2$ single phase (measured composition: $La_{19.4}Mg_{42.4}Sn_{38.2}$) with a small amount of Mg_2Sn.

Results of EDXS analysis of the two title phases found in several samples annealed at 500 °C [15] are listed in Table 2, showing a detectable homogeneity range for both.

Table 2. Measured compositions of the phases $La_3Mg_{4-x}Sn_{2+x}$ (samples A1-A8) and $LaMg_{3-x}Sn_2$ (samples B1-B8).

Sample code – global composition (at.%)	EDXS Composition $La_3Mg_{4-x}Sn_{2+x}$ (at.%) La; Mg; Sn	Sample code – global composition (at.%)	EDXS Composition $LaMg_{3-x}Sn_2$ (at.%) La; Mg; Sn
A1 –$La_{35.8}Mg_{38.1}Sn_{26.1}$	34.7; 40.0; 25.3	B1 – $La_{23.3}Mg_{40.0}Sn_{36.7}$	19.9; 42.5; 37.6
A2 – $La_{33.2}Mg_{33.5}Sn_{33.3}$	34.6; 40.5; 24.9	B2 – $La_{13.9}Mg_{48.9}Sn_{37.2}$	19.1; 42.9; 38.0
A3 – $La_{13.9}Mg_{82.0}Sn_{4.1}$	34.4; 41.5; 24.1	B3 – $La_{6.2}Mg_{58.5}Sn_{35.3}$	18.4; 45.3; 36.3
A4 – $La_{33.8}Mg_{46.0}Sn_{20.2}$	34.8; 41.7; 23.5	B4 – $La_{23.0}Mg_{41.4}Sn_{35.6}$	18.5; 45.7; 35.8
A5 – $La_{20.0}Mg_{76.7}Sn_{3.3}$	34.5; 42.0; 23.5	B5 – $La_{8.1}Mg_{72.1}Sn_{19.8}$	18.2; 46.1; 35.7
A6 – $La_{23.7}Mg_{70.5}Sn_{5.8}$	34.5; 42.4; 23.1	B6 – $La_{8.0}Mg_{77.4}Sn_{14.6}$	18.3; 46.3; 35.4
A7 – $La_{33.0}Mg_{47.6}Sn_{19.4}$	34.8; 42.4; 22.8	B7 – $La_{16.6}Mg_{49.3}Sn_{34.1}$	17.8; 47.1; 35.1
A8 – $La_{29.6}Mg_{59.9}Sn_{10.5}$	34.9; 42.9; 22.2	B8 – $La_{2.5}Mg_{88.3}Sn_{9.2}$	17.9; 47.6; 34.5

3.2 Crystal structure of $La_3Mg_{4-x}Sn_{2+x}$

The indexing of the diffraction dataset of $La_3Mg_{4-x}Sn_{2+x}$ single crystal gives a small hexagonal unit cell with $a = 7.80$ Å, $c = 4.48$ Å. The collected reflection conditions are compatible with several space groups: *P*6, $P\bar{6}$, *P*6/*m*, *P*622, *P*6*mm*, $P\bar{6}2m$ and *P*6/*mmm*. The structure solution was easily found in $P\bar{6}2m$ with the aid of the charge flipping algorithm implemented in Jana2006 [17]. No chemically sound models were found in other space groups.

The deduced preliminary structural model contains four crystallographic sites, giving the $La_3Mg_4Sn_2$ formula and corresponding to the $Zr_3Cu_4Si_2$ prototype. Nevertheless, this model is not completely in agreement with some observations: the EDXS measured composition of the studied phase slightly deviates from the exact 3:4:2 ratio and the isotropic thermal parameter for Mg in the 1*a* site is too big compared with other species. At this point, a Mg/Sn statistical mixture was refined

in this position, drastically reducing the residual values and giving the more reliable $La_3Mg_{4-x}Sn_{2+x}$ (x = 0.12(1)) model. In the next cycles of refinement, all the atom sites were refined anisotropically, except the Mg/Sn 1*a* site, for which these parameters were constrained to be identical. Refinement of the correct absolute structure of $La_3Mg_{4-x}Sn_{2+x}$ was ensured through calculation of the Flack parameter.

Results of Rietvel refinement on sample #1 are visualized in figure 2: among the known secondary phases identified by SEM-EDXS analysis only $LaMg_3$ was detected in the experimental diffraction pattern, possibly due to the sample inhomogeneity or to a small content of other phases. A narrow angular range (30-32°), containing unindexed reflections of weak intensity, was excluded from the refinement. Least-squares refinement cycles converged to $R_F = 0.070$ and $R_B = 0.102$ for the main phase, indicating that the diffraction pattern calculated on the basis of the established structural model of $La_3Mg_{4-x}Sn_{2+x}$ is in a good agreement with the experimental data. The refined abundance of the phase of interest is 53 wt%. The refined lattice parameters, atomic positions and Mg/Sn statistical mixture are in acceptable agreement with single crystal data, which are listed in Table 3 and will be considered for further discussion. The interatomic distances listed in Table 3 do not deviate noticeably from the atomic radii sum.

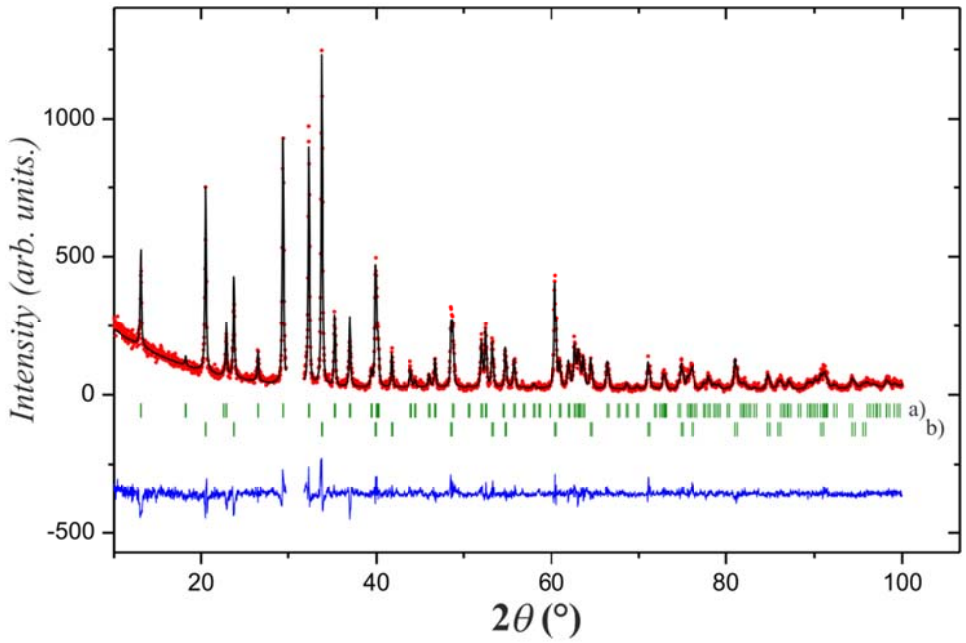

Figure 2. Observed (red circles), calculated (black line) and difference (bottom blue line) X–ray powder diffraction patterns for sample #1 ($La_{35.0}Mg_{43.0}Sn_{22.0}$). Vertical bars indicate the Bragg positions of corresponding phases: $La_3Mg_{4-x}Sn_{2+x}$ (a) and $LaMg_3$ (b).

Table 3. Atomic coordinates, equivalent isotropic displacement parameters and interatomic distances for the $La_3Mg_{4-x}Sn_{2+x}$ single crystal.

Atom	**Wyck. site**	**Site**	***x/a***	***y/b***	***z/c***	**SOF≠1**	**U_{eq}, Å^2**
La1	3*f*	*m*2*m*	0.57499(5)	0	0		0.0114(1)
Sn1	2*d*	-6..	1/3	2/3	1/2		0.0104(1)
Mg1	3*g*	*m*2*m*	0.2434(3)	0	1/2		0.0156(6)
Mg2	1*a*	-62*m*	0	0	0	0.88(1)	0.0147(9)
Sn2	1*a*	-62*m*	0	0	0	0.12(1)	0.0147(9)
Interatomic distances							
	Central atom	**Adjacent atoms**	***d* (Å)**	**Central atom**	**Adjacent atoms**	***d* (Å)**	
	La1–	Mg2	3.314(1)	Mg1–	2Sn1	3.011(2)	
		4Sn1	3.356(1)		2Mg2	3.075(1)	
		2Mg1	3.541(2)		2Mg1	3.287(3)	
		4Mg1	3.761(1)		2La1	3.541(2)	
	Sn1–	Mg1	3.011(2)		4La1	3.761(1)	
		2Mg1	3.012(2)	Mg2–	6Mg1	3.075(1)	
		6La1	3.356(1)		3La1	3.314(1)	

The $La_3Mg_{4-x}Sn_{2+x}$ belongs to the *hP*9-$Zr_3Cu_4Si_2$ prototype, with only a few representatives of general formula $(Zr,Hf)_3Cu_4(Si,Ge)_2$ [23] known up to now. A partial Mg/Sn substitution was observed in the studied crystal, in agreement with EDXS data. A narrow homogeneity range, extending from about x = 0.12 to x = 0.40, was observed for this phase at 500 °C (see Table 2). It could be highlighted that the homogeneity region does not reach the exact 3:4:2 stoichiometry.

The title phase can be viewed as an ordered derivative of the *hP*9-ZrNiAl prototype, very common for chemically similar equiatomic ternary compounds. It is worth noticing that the LaMgSn compound also exists, crystallizing in the related *oP*12-TiNiSi structure type [14]. More details on structural relations between the known La–Mg–Sn ternary compounds are reported and discussed in paragraph 3.4.

3.3 Crystal structure of $LaMg_{3-x}Sn_2$

The indexation of the collected single-crystal dataset of $LaMg_{3-x}Sn_2$ was straightforward, giving a hexagonal unit cell with *a* = 8.32 Å, *c* = 14.954 Å. The systematic absences analysis indicated only two possible trigonal space groups: $P\bar{3}1c$ (No. 163) or *P*31*c* (No. 159). This result, joined with the fact that the measured EDXS composition of this compound is very close to that of the $LaMg_{3-x}Ge_2$ phase recently found in the La–Mg–Ge ternary system [3], strongly suggests these two intermetallics being isostructural. The first cycles of least squares structural refinement confirmed this, showing good residual values and an acceptable difference Fourier map for the "$La_3Mg_8Sn_6$" model, corresponding to $LaMg_{3-x}Sn_2$ with x = 1/3. Some of the weak super-reflections characteristic

of this ordered superstructure are visible also in the precession photo shown in fig. 1b. Considering the detected homogeneity range at the studied conditions (see Table 2), the site occupancy parameter (SOF) was left to vary for all the atom sites, but only SOF for Mg localized in the 2*a* Wyckoff position shows a slight deviation from the unity value (being ~0.95). The final structure model was refined with the anisotropic displacement parameters for all crystallographic sites, converging at *w*R2 = 0.019 and GOF = 1.12.

Results of Rietveld refinement on sample #2 are visualized in figure 3: the diffraction pattern calculated on the basis of the established structural model of $LaMg_{3-x}Sn_2$ fits pretty well with the experimental data (R_F = 0.057, R_B = 0.048), considering Mg_2Sn as secondary phase. The refined abundance of the main phase is 95 wt%, in agreement with the SEM observation.

The refined lattice parameters and atomic positions are in acceptable agreement with single crystal data, which are listed in Table 4 and will be considered for further discussion.

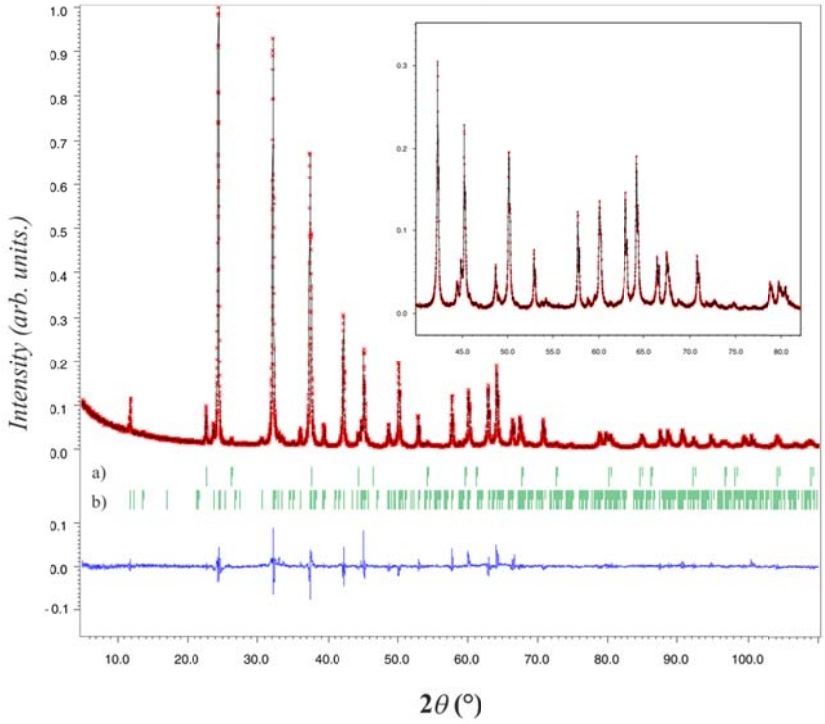

Figure 3. Observed (red crosses), calculated (black line) and difference (bottom blue line) X–ray powder diffraction patterns for sample #2 ($La_{17.0}Mg_{48.0}Sn_{35.0}$). Vertical bars indicate the Bragg positions of corresponding phases: Mg_2Sn (a) and $LaMg_{3-x}Sn_2$ (b). The inset shows a zoom of the 40-82 range of the pattern.

The obtained x value (0.35) is in fair agreement with the "theoretical" value x=1/3, corresponding to the "3:8:6" superstructure of the $LaLi_3Sb_2$-type described for the $LaMg_{3-x}Ge_2$ prototype [3]. The slightly different Mg concentration arises from a partial occupation (SOF = 0.95) of the 2*a* site by Mg atoms.

Even if the $LaLi_3Sb_2$ prototype has not many representatives, hundreds of ternary compounds are isostructural with its defect derivative $CaAl_2Si_2$ type [23]; the $LaMg_{3-x}Tt_2$ ($x \approx 1/3$, *Tt* = Ge, Sn) compounds can be considered as the first members of a new group of $LaLi_3Sb_2$ defective derivatives. The group-subgroup relation between the $LaLi_3Sb_2$ parent type and the $\sqrt{3}a \times \sqrt{3}a \times 2c$ superstructure of formula $LaMg_{3-x}Tt_2$ ($x \approx 1/3$, *Tt* = Ge, Sn) is shown in fig. 4a. This scheme, already used when deducing the correct structure for the prototype with Ge [3], is reported here with the purpose to discuss the $LaMg_{3-x}Sn_2$ off-stoichiometry from the geometrical point of view.

Similarly to $LaLi_3Sb_2$ and $CaAl_2Si_2$ types, the crystal space of $LaMg_{3-x}Tt_2$ can be viewed as composed of slabs containing only Mg and *Tt* atoms well separated by flat layers of La atoms (see Fig. 4b). Each unit cell contains two such slabs related by the inversion symmetry operator at 1/2 1/2 1/2.

Table 4. Atomic coordinates, equivalent isotropic displacement parameters and interatomic distances for the $LaMg_{3-x}Sn_2$ single crystal.

Atom	**Wyck. site**	**Site**	***x/a***	***y/b***	***z/c***	**SOF≠1**	**U_{eq}, Å^2**
La1	2*b*	-3..	0	0	0		0.0105(1)
La2	4*f*	3..	1/3	2/3	0.00063(2)		0.0108(1)
Sn1	12*i*	1	0.01557(2)	0.33477(2)	0.12518(2)		0.0122(1)
Mg1	12*i*	1	0.35854(12)	0.02639(12)	0.32610(7)		0.0182(2)
Mg2	2*c*	3.2	1/3	2/3	1/4		0.0183(5)
Mg3	2*a*	3.2	0	0	1/4	0.94(1)	0.0183(8)

Interatomic distances

	Central atom	**Adjacent Atoms-**	***d* (Å)**	**Central atom**	**Adjacent atoms**	***d* (Å)**
	La1–	6Sn1	3.305(1)	Mg1–	Sn1	2.839(1)
		2Mg3	3.739(1)		Sn1	2.840(1)
		6Mg1	3.881(1)		Sn1	2.956(1)
	La2–	2Sn1	3.284(1)		Sn1	3.024(1)
		Sn1	3.285(1)		Mg3	3.097(1)
		3Sn1	3.455(1)		Mg2	3.110(1)
		1Mg1	3.655(1)		Mg1	3.414(1)
		2Mg1	3.656(1)		Mg1	3.436(1)
		Mg2	3.729(1)		La2	3.656(1)
		3Mg1	3.885(1)		La1	3.881(1)
	Sn1–	Mg1	2.839(1)		La2	3.885(1)
		Mg1	2.840(1)		Mg1	3.930(1)
		Mg1	2.956(1)	Mg2–	4Mg1	3.110(1)
		Mg1	3.024(1)		2Mg1	3.111(1)
		La2	3.284(1)		2Sn1	3.286(1)
		Mg2	3.287(1)		4Sn1	3.287(1)
		Mg3	3.302(1)		2La2	3.729(1)
		La1	3.305(1)	Mg3–	6Mg1	3.097(1)
		La2	3.455(1)		6Sn1	3.302(1)
					2La1	3.739(1)

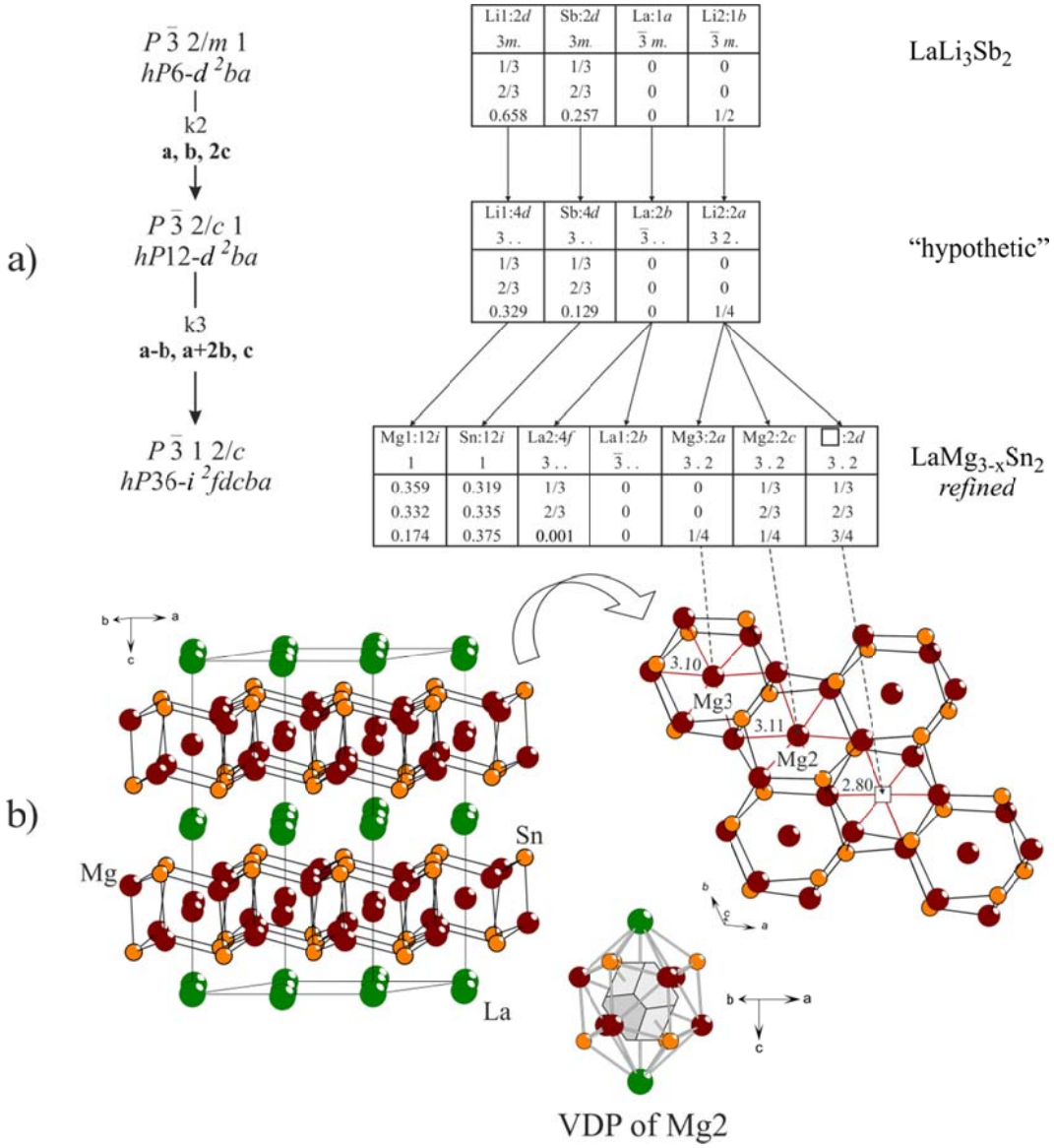

Fig. 4. a) Group-subgroup relation in the *Bärnighausen* formalism for the $LaLi_3Sb_2$ and $LaMg_{3-x}Sn_2$ structures. The indexes of the symmetry reductions and the evolution of the atomic parameters are given; b) Crystal structure of $LaMg_{3-x}Sn_2$ viewed along the (001) direction (left part); puckered layer of Mg and Sn atoms hosting Mg2, Mg3 and vacancy □ (right part). As an example, the Voronoi polyhedron (VDP) of Mg2 is shown.

The further discussion will refer particularly to the $LaMg_{3-x}Sn_2$ phase, but analogous considerations can be extended to the Ge-containing prototype.

The analysis of interatomic distances distribution and number of contacts within the Mg–Sn buckled slabs allows to clearly distinguishing between Mg species, inducing to think on different chemical roles of Mg.

Four shortest Mg–Sn contacts, ranging from 2.84÷3.02 Å and resulting in a somewhat elongated tetrahedron, are established by Mg and Sn of general symmetry sites, characterized also by the biggest absolute shift with regard to Li/Sb pairs in the $LaLi_3Sb_2$ type (see fig. 4a).

Each of the tetrahedra shares four adjacent edges with neighbouring tetrahedra (for details see [24]) giving a robust framework. It should be noted that the strongest Mg–Sn contacts in other ternary compounds showing similar Mg–Sn slabs, such as Na_2MgSn [25] and LaMgSn [26], are likewise distanced.

Within this Mg–Sn network three distorted hexagonal cavities can be highlighted, with centres of mass corresponding to 2*c* (fully occupied by Mg2), 2*a* (partially occupied by Mg3) and 2*d* (vacant) Wyckoff sites. All these sites are more than 3 Å apart from the closest Sn atoms. The relative volumes of these cavities can be estimated applying the geometrical concept of Voronoi-Dirichlet polyhedra (VDP) analysis [27] accounting for all contacts of central atoms within the first coordination sphere. The volumes of VDP were estimated with the help of Dirichlet program implemented into ToposPro package [28], considering solid angles to be bigger than 3 º for Voronoi crystal space partitioning. It was found that the volume of VDP of Mg2 is 23.18 $Å^3$ (2*c*, SOF=1), of Mg3 is 23.18 $Å^3$ (2*a*, SOF=0.95) and only 20.29 $Å^3$ for the vacant position (2*d*).

The point symmetry of the 2*a*, 2*c*, 2*d* sites is the same – 3.2, as well as the respective atomic arrangement consisting of 14 atoms (of $[Mg/□@La_2Mg_6Sn_6]$ composition). The corresponding VDP for other atoms correlates well with their size in this compound: La1 (31.18 $Å^3$), La2 (31.46 $Å^3$), Sn (24.96 $Å^3$).

Coherent results can be obtained analyzing the Mg–Mg/ Mg–□ distances. The Mg2 atoms have six Mg atoms equidistanced at 3.11 Å. It is somewhat shorter than the 3.2 Å distanced Mg–Mg contacts in *hcp* Mg, although frequently found in Mg-rich compounds [29]. The Mg3 atoms are coordinated by six Mg atoms at a similar distance of 3.10 Å. The last 2*d* site is positioned too close to Mg from the strongly bonded network (2.80 Å), thus, remaining vacant (See Fig. 4b, right). Such a simple geometric reasoning agrees well with the experimentally observed off-stoichiometry of the $LaMg_{3-x}Sn_2$ compound.

On the other hand, this phase was found to exist in the homogeneity range from $x \approx 0.33$ to $x \approx 0.78$ (see Table 2). The Mg poorer compositions ($x>0.33$) can be structurally supported by a smaller occupation degree of the 2*a* site. In fact, even in the Ge prototype, the SOF of the same site is only 0.78 [3].

3.4 Structural relationships between La–Mg–Sn ternaries

The three La–Mg–Sn compounds known so far (LaMgSn, $La_3Mg_{4-x}Sn_{2+x}$ and $LaMg_{3-x}Sn_2$) enrich the family of structures related by symmetry reduction to the AlB_2-aristotype. A convenient way to represent the symmetry relations inside a family of compounds is the *Bärnighausen* formalism, developed within the group theory. This approach is not only descriptive, but it also helps to highlight and explain a number of phenomena causing symmetry reduction, such as vacancy formation, bonding interactions between atoms, ordered occupancy of equivalent sites by different species, and many others [30]. The group-subgroup relations tool was applied by Hoffmann and Pöttgen to construct a big tree including both the hexagonal/trigonal and orthorhombic/monoclinic derivatives of the AlB_2-type [31]. Some branches were subsequently added with the discovery of new compounds [32].

The $LaMg_{3-x}Tt_2$ themselves represent a new branch of the hexagonal derivatives inside the AlB_2-tree, instead LaMgSn and $La_3Mg_{4-x}Sn_{2+x}$ find their place within the original chart, in the orthorhombic and hexagonal groups, respectively. A reduced version of the AlB_2 *Bärnighausen* tree including the compounds of interest is shown in fig. 5, complemented with structure representations highlighting their relations. In the studied La–Mg–Sn ternary compounds three-dimensional Mg–Sn frameworks are evidenced, deriving from different distortions/colouring of the 2D planar three-connected boron network of the AlB_2 parent type. The existence of such networks formed by magnesium and tetrel elements was recently proposed for a number of compounds also on the basis of chemical bonding studies [7, 10, 33]. On the other hand, La atoms mainly play the role of spacers, which is reflected in a less distorted pattern with respect to the aristotype.

As it was already introduced in paragraph 3.2, the $La_3Mg_{4-x}Sn_{2+x}$ (*hP*9, ordered derivative of the ZrNiAl prototype) and LaMgSn (*oP*12-TiNiSi) also represent two structural modifications very common for equiatomic ternaries. Different driving forces for the formation of the former or the latter were studied. For example, higher temperature and pressure favor the hexagonal polimorph for YbPdSn [34] and CePtSn [35], respectively.

The electronegativity also can act as a key factor stabilizing one of the two structures. This is the case of the CaAg*Pn* (*Pn* = As, Sb) compounds: for *Pn* = As the ZrNiAl type realizes, instead for *Pn* = Sb the TiNiSi-like structure forms, as a consequence of the different degree of polarity of the Ag-*Pn* bonds [23, 36]. On the other hand, the different nature of one of the components may lead to the formation of new structures, being intergrown derivatives of the discussed prototypes [36].

Another case is represented by the above mentioned stannides, where the chemical pressure induced by the different Mg/Sn ratio determines the stability of the hexagonal or the orthorhombic structure. A similar situation occurs in the (Zr, Hf)–Cu–(Si, Ge) systems [23].

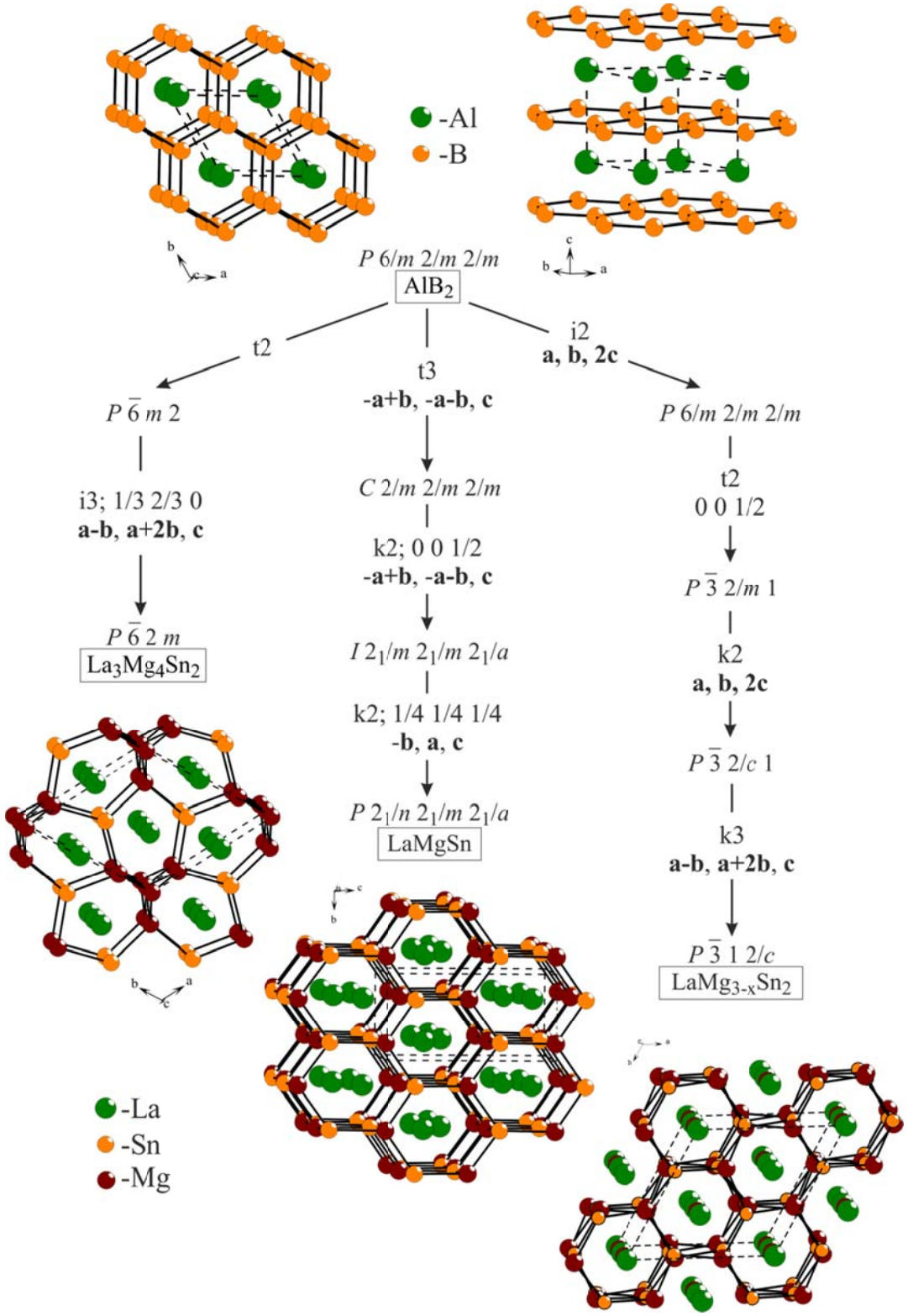

Figure 5. *Bärnighausen* tree of the group-subgroup relationships of the AlB_2 type and its La-Mg-Sn ternary derivatives. The types (k, t, i) and indices (integer numbers) of the symmetry reduction steps are given together with the unit cell transformations and origin shifts. Cutouts of the structures of interests are also shown. More details on the structures of intermediate steps can be found in [31, 32].

4. Conclusion

The crystal structures of the two novel compounds $La_3Mg_{4-x}Sn_{2+x}$ ($0.12 \leq x \leq 0.40$, *hP*9-$Zr_3Cu_4Si_2$) and $LaMg_{3-x}Sn_2$ ($0.33 \leq x \leq 0.78$, *hP*34-0.12, $LaMg_{3-x}Ge_2$) were studied by single crystal and powder X-ray diffraction techniques. The off-stoichiometry of the studied phases has different origins: for the former it is due to Mg/Sn statistical mixture, for the latter it arises from Mg/□ ordering.

Basing on literature data on related compounds and on the analysis of interatomic distances, the crystal spaces of the $La_3Mg_{4-x}Sn_{2+x}$, $LaMg_{3-x}Sn_2$ and LaMgSn phases could be presented as composed of a Mg–Sn network hosting La atoms. These structures are strictly related, since they can be derived through symmetry reduction from the common AlB_2 aristotype, taking place on different branches of the corresponding *Bärnighausen* tree. Loss of symmetry elements is mainly caused by the Mg–Sn network deformation; instead the La atoms pattern remains less distorted.

The flexibility of the Mg–Sn framework depends on several factors, such as concentration of constituents and their electronegativity difference: this motivates us to investigate the effects of La substitution by other rare earth metals on phase formation and crystal structures in R–Mg–Sn systems.

Acknowledgements

This research has been supported by the University of Genoa, within PRA 2014 projects.

DMP acknowledges the Ministry of Education and Science of Russia (grant 14.B25.31.0005).

References

[1] S. De Negri, P. Solokha, A. Saccone, V. Pavlyuk, *Intermetallics* 17 (2009) 614–621.

[2] S. De Negri, P. Solokha, V. Pavlyuk, A. Saccone, *Intermetallics* 19 (2011) 671-681.

[3] S. De Negri, P. Solokha, M. Skrobańska, D.M. Proserpio, A. Saccone, *J. Solid State Chem.* 218 (2014) 184-195.

[4] U. Ch. Rodewald, B. Chevalier, R. Pöttgen, *J. Solid State Chem.* 180 (2007) 1720–1736.

[5] P. Solokha, S. De Negri, V. Pavlyuk, A. Saccone, *Inorg. Chem.* 48 (2009) 11586–11593.

[6] P. Solokha, S. De Negri, V. Pavlyuk, B. Eck, R. Dronskowski, A. Saccone, *J. Sol. State Chem.* 183 (2010) 2995–3001.

[7] P. Solokha, S. De Negri, M. Skrobanska, A. Saccone, V. Pavlyuk, D.M. Proserpio, *Inorg. Chem.* 51 (2012) 207−214.

[8] P. Solokha, S. De Negri, V. Pavlyuk, A. Saccone, G. Fadda, *Eur. J. Inorg Chem.* (2012) 4811-4821.

[9] T. Block, M. Johnscher, S. Linsinger, U. Ch. Rodewald, R. Pöttgen, *Z. Naturforsch.* 70(2) b (2015) 135–141.

[10] H. Allescher-Last, H.-U. Schuster, *Z. Naturforsch.* 48b (1993) 240-242.

[11] W. Choe, G.J. Miller, E.M. Levin, *J. Alloys Compd.* 329 (2001) 121-130.

[12] R. Kraft, R. Pöttgen, Monatsh. Chem. 135 (2004) 1327–1334.

[13] N.-T. Suen, S. Bobev, *Eur. J. Inorg. Chem.* (2012) 4141-4148.

[14] P. Manfrinetti, A. Provino, K.A. Gschneidner Jr., *J. Alloys Compds* 482 (2009) 81–85.

[15] S. De Negri, P. Solokha, R. Minetti, M. Skrobańska, A. Saccone, manuscript in preparation

[16] Bruker (2014). *APEX2*, *SAINT-Plus*, *XPREP*, *SADABS*. Bruker AXS Inc., Madison, Wisconsin, USA.

[17] V. Petříček, M. Dušek, L. Palatinus, *Z. Kristallogr.* 229(5) (2014) 345-352.

[18] G.M. Sheldrick, *Acta Cryst. A* 64 (2008) 112-122.

[19] L.J. Farrugia, *J. Appl. Cryst.* 45 (2012) 849-854.

[20] A.L. Spek PLATON, a multipurpose crystallographic tool. Utrecht University, The Netherlands, 2002

[21] L.Gelato, E. Parthé, *J. Appl. Crystallogr.* 20 (1987) 139-143.

[22] J. Rodriguez-Cavajal, "Recent developments in the program FullProf", Newsletter 26 (2001) 12-19.

[23] P. Villars, K. Cenzual, Pearson's Crystal Data, Release 2014/15, ASM International, Ohio, USA**.**

[24] C. Zheng, R. Hoffman, R. Nesper, H.-G. Schnering, *J. Am. Chem. Soc.* 108 (1986) 1876-1884.

[25] T. Yamada, V.L. Deringer, R. Dronskowski, H. Yamane, *Inorg. Chem.* 51 (2012) 4810−4816.

[26] P. Manfrinetti, A. Provino, K.A. Gschneidner, *J. Alloys Compds* 482 (2009) 81–85.

[27] V.A. Blatov, *Crystallogr. Rev.* 10 (2004) 249–318.

[28] V.A. Blatov, A. P. Shevchenko, D.M. Proserpio, *Cryst. Growth Des.* 14 (2014) 3576-3586.

[29] P. Solokha, S. De Negri, V. Pavlyuk, A. Saccone, *Solid State Sci.* 11 (2009) 801-811.

[30] Müller U. *Symmetry Relationships between Crystal Structures. Applications of Crystallographic Group Theory in Crystal Chemistry*, Oxford University Press, 2013.

[31] R.-D. Hoffmann, R. Pöttgen, *Z. Kristallogr.* 216 (2001) 127–145.

[32] V. Hlukhyy, T.F. Fässler, *Z. Anorg. Allg. Chem.* 634 (2008) 2316-2322.

[33] T. Yamada, V. L. Deringer, R. Dronskowski, H. Yamane, *Inorg. Chem.* 51 (2012) 4810−4816.

[34] D. Kußmann, R. Pöttgen, B. Künnen, G. Kotzyba, R. Müllmann, B.D. Mosel, *Z. Kristallogr.* 213 (1998) 356-363.

[35] J.F. Riecken, G. Heymann, T. Soltner, R.-D. Hoffmann, H. Huppertz, D. Johrendt, R. Pöttgen, *Z. Naturforsch.* 60b (2005) 821-830.

[36] S. Ponou, S. Lidin, *Z. Anorg. Allg. Chem.* 635 (2009) 2143-2146.